Letter

Microscopic mechanism of displacive excitation of coherent phonons in a bulk Rashba semiconductor

P. Fischer,[1] J. Bär,[1] M. Cimander,[1] L. Feuerer,[1] V. Wiechert,[1] O. Tereshchenko,[2] and D. Bossini[1]
[1]*Department of Physics and Center for Applied Photonics, University of Konstanz, D-78457 Konstanz, Germany*
[2]*Rzhanov Institute of Semiconductor Physics, Siberian Branch, Russian Academy of Sciences, Novosibirsk 630090, Russia*

(Received 11 October 2024; revised 23 December 2024; accepted 22 January 2025; published 4 February 2025)

Changing the macroscopic properties of quantum materials by optically activating collective lattice excitations has recently become a major trend in solid state physics. One of the most commonly employed light-matter interaction routes is the displacive mechanism. However, the fundamental contribution to this process remains elusive, as the effects of free-carrier density modification and raised effective electronic temperature have not been disentangled yet. Here we use time-resolved pump-probe spectroscopy to address this issue in the Rashba semiconductor BiTeI. Exploring the conventional regime of electronic interband transitions for different excitation wavelengths as well as the barely accessed regime of electronic intraband transitions, we answer this question regarding the displacive mechanism: the lattice modes are predominantly driven by the rise of the effective electronic temperature. In the intraband regime, which allows an increase of the effective carrier temperature while leaving the carrier density unaffected, the phonon coherence time does not display significant fluence-dependent variations. Our results thus reveal a pathway to displacive excitation of coherent phonons, free from additional scattering and dissipation mechanisms typically associated with an increase of the free-carrier density.

DOI: 10.1103/PhysRevB.111.L081201

Introduction. The generation of coherent phonons through laser pulses has recently been established as a means to both control [1–4] and probe [5,6] the macroscopic phases of quantum materials. Impulsive non-resonant processes are one of the most popular approaches to the optical excitation of coherent lattice dynamics. In particular, they allow the excitation of longitudinal optical (LO) phonons which are symmetrically inaccessible to resonant dipolar excitation. In general, a distinction is drawn between two methods: If light couples to the electronic system nonresonantly, coherent phonons are induced by impulsive stimulated Raman scattering. On the other hand, if the optical stimulus is resonant with the electronic system, displacive excitation of coherent phonons (DECP) is realized [7,8]. Within the framework of the established theory of DECP [9] the electronic system absorbs the pump beam and subsequently thermalizes internally, on a timescale short compared to the phonon period. The excited electronic system induces a displacement of the quasi-equilibrium nuclear coordinate which results in coherent lattice vibrations. The theory attributes the generation of coherent phonons to two contributions, namely the increase of the charge-carrier density n_c and the rise in the effective temperature of the electronic subsystem T_e. Crucially for our work, the theory can neither quantitatively disentangle the two contributions nor assess which one is the dominant drive for the phonon excitation. Numerical modeling in the case of bismuth [10] has attributed the displacive mechanism to an increase in n_c. This interpretation is further supported by x-ray diffraction measurements [11]. However, these experiments were performed by optically exciting interband transitions. Therefore, in the absorption process both n_c and T_e are increased. Modern laser sources can emit femtosecond pulses in the mid-infrared regime, with photon energies lower than the band gap of most solids. Mid-infrared laser pulses can therefore be employed to pump electronic intraband transitions selectively, which raises only T_e and keeps n_c constant. Notably, THz (0–5 THz) laser pulses have been recently employed to drive coherent phonons by pumping electronic intraband transitions [12]. The mechanism enabling the generation of collective lattice excitations was ascribed to a coupling between the phonons and the sum frequency of different components of the pump beam [12]. This route of light-matter interaction is different from the mechanism underlying DECP, which is based on coupling the difference frequency of components of the pump beam to the lattice [13,14]. Importantly, the experimental condition required for the impulsive excitation of the electronic system in the DECP process involves pump pulses with a duration shorter than the phonon oscillation period. This condition is not met in the recent THz experiment [12], where the pulse duration exceeds the phonon period. Therefore, investigating the microscopic mechanism of DECP requires mid-infrared laser pulses, able to induce intraband transitions, with a duration shorter than the phonon oscillation period.

We explore the excitation of coherent phonons in BiTeI, a prototypical Rashba semiconductor, via pump-probe time-domain spectroscopy. The band structure of this material is ideal for a quantitative comparison of interband and intraband DECP. Due to the narrow band gap, BiTeI absorbs light in the near-infrared spectral range via electronic interband transitions. The high intrinsic carrier

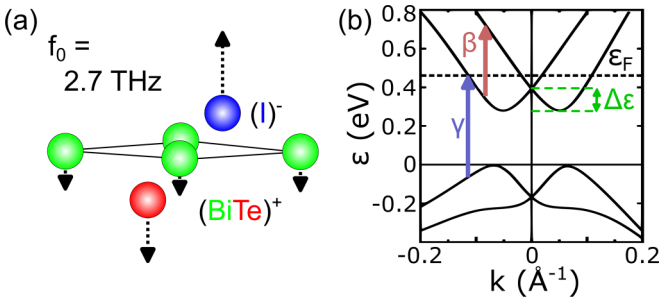

FIG. 1. (a) Atomic displacement and central frequency of an A_1 phonon mode in BiTeI [20]. (b) Rashba-split band structure of BiTeI (adapted from [26]; $\Delta\varepsilon = 100$ meV). The transition β (red dashed line at 0.37 eV) represents the highest-energy intraband transition. The transition γ (blue dashed line at 0.52 eV) is the lowest-energy interband transition corresponding to the electronic excitation from the valence band to a free state above the Fermi energy ε_F (dashed black line).

density combined with the huge Rashba spin splitting ($\Delta\varepsilon \approx 100$ meV) of the lowest conduction band allows intraband transitions in the mid-infrared regime [15].

Our experiments reveal that in the interband regime the phonon coherence time is not affected up to an optically doped carrier density of $n_c \approx 1 \times 10^{21}$ cm^{-3}. These findings demonstrate that BiTeI is a surprisingly robust material for coherent phononics. This result is remarkable, considering that in other semiconductors (GaAs, GaP, InAs, InSb) the coherence time is typically suppressed by carrier densities orders of magnitude smaller than in BiTeI [16–19]. Strikingly in the intraband regime the amplitude of the phonons linearly increases with the laser fluence, even though n_c remains constant. Even more tantalizing, the phonon coherence time remains unaffected, even if the laser fluence is set to a value one order of magnitude higher than in the case of electronic interband pumping.

Materials and methods. Our BiTeI specimen was grown by a modified Bridgman method using a rotating heat field [15]. Its layered structure is built from covalently bound bilayers formed by $(BiTe)^+$ which ionically bond to $(I)^-$ and thus form trilayers. These trilayers in turn are stacked by van der Waals forces. We are investigating interband and intraband DECP in BiTeI via pump-probe time-domain reflection spectroscopy. Therefore, we are interested in phonons with A_1 symmetry [9]. As demonstrated by spontaneous Raman scattering [20], BiTeI features an A_1 mode at a center frequency of 2.7 THz. Its corresponding atomic displacement is shown in Fig. 1(a). For our experiments, we employ two different amplified laser systems emitting femtosecond pulses at kHz repetition rates (details in [21]). A commercial system delivers laser pulses with a central photon energy tunable in the visible and near-infrared ranges (0.5 eV to 3 eV, 2 μm to 400 nm). A self-built system [22] generates pulses in the mid-infrared (0.18 eV, 7.0 μm). Thus, we are able to employ photon energies both above and below the fundamental band gap of BiTeI (band-gap energy $\varepsilon_g \approx 0.38$ eV [23]). In all our experiments, the central wavelength of the probe beam is 1.2 μm (photon energy ≈ 1 eV). The reflected probe beam is recollected and detected by two photodiodes in a balanced detection scheme. The signal is acquired via a digital lock-in method. The sample was always at room temperature.

Figure 1(b) depicts the electronic band structure of BiTeI. The compound is classified as a degenerate n-type semiconductor, implying that its Fermi energy ε_F lies above the conduction-band minimum [23] (black dashed line). Because of the Rashba effect [24], the dispersion of electrons with antiparallel spins is displaced in opposite directions from the center of the Brillouin zone. The resulting energy splitting measured from the bottom of the conduction bands to their intersection is $\Delta\varepsilon \approx 100$ meV (green dashed lines) [23]. Consequently, the absorption properties are characterized by two electronic transitions. With β we represent the highest-energy intraband transition between the Rashba-split conduction bands [25] (red arrow). The lowest-energy interband transition, promoting electrons from the highest valence band to an unoccupied state above ε_F in the lowest conduction band, is denoted by γ (blue arrow). To determine the energies of these two transitions we measure the transmission spectrum of our sample (details in [21]) and obtain $\beta = 0.37$ eV (3.35 μm) and $\gamma = 0.52$ eV (2.39 μm). Depending on the crystal-growth conditions, the intrinsic charge-carrier density n_i of BiTeI can vary considerably. Since γ depends on ε_F, it is sensitive to n_i. Comparing the experimentally obtained value of γ to the literature [27], we estimate the intrinsic carrier density in our sample to be $n_i = 6 \times 10^{19}$ cm^{-3}.

Results and discussion. The main scientific goal of our work is to unravel the microscopic nature of DECP. We begin with the canonical regime of the displacive mechanism, in which the excitation of electronic interband transitions increases both n_c and T_e.

Figure 2(a) shows the dynamics of the normalized transient reflectivity $\Delta R/R_0$ induced by laser pulses with a central wavelength of 520 nm. The pulse duration is 200 fs and the fluence is set to $\Phi = 1.39$ mJ/cm^2. The signal consists of two components, (i) harmonic oscillations with a period on the femtosecond timescale superimposed on (ii) an exponential decay on the picosecond timescale with an amplitude of $\Delta R/R_0 \approx 1.5 \times 10^{-2}$. Calculating the power spectrum via Fourier transform [Fig. 2(b)] reveals that the central frequency of the oscillations is 2.76 THz, a value consistent with the A_1 mode, whose atomic displacement corresponds to the out-of-phase oscillations of $(BiTe)^+$ and $(I)^-$ [20] [Fig. 1(a)]. We ascribe the exponential contribution to the signal to the thermalization of the photoexcited electrons with acoustic phonons [28].

Analyzing the isolated oscillatory component of $\Delta R/R_0$ [details in [21]; green circles in Fig. 2(c)], we obtain that the amplitude of the oscillations amounts to approximately 0.72×10^{-3}. Assuming a δ-function temporal profile, the signatures in $\Delta R(t)/R_0$ could be described in the time domain by damped oscillations represented by the following equation [9]:

$$\left(\frac{\Delta R(t)}{R_0}\right)_{\text{osci}} = A_o \exp\left(-\frac{t}{\tau}\right)\cos(2\pi f_0 t)\Theta(t). \quad (1)$$

Here, A_o is the amplitude, τ the lifetime of the oscillations, f_0 the central frequency, and $\Theta(t)$ the Heaviside function. However, since the duration of the pump pulses is almost comparable with the period of the mode, the onset of the

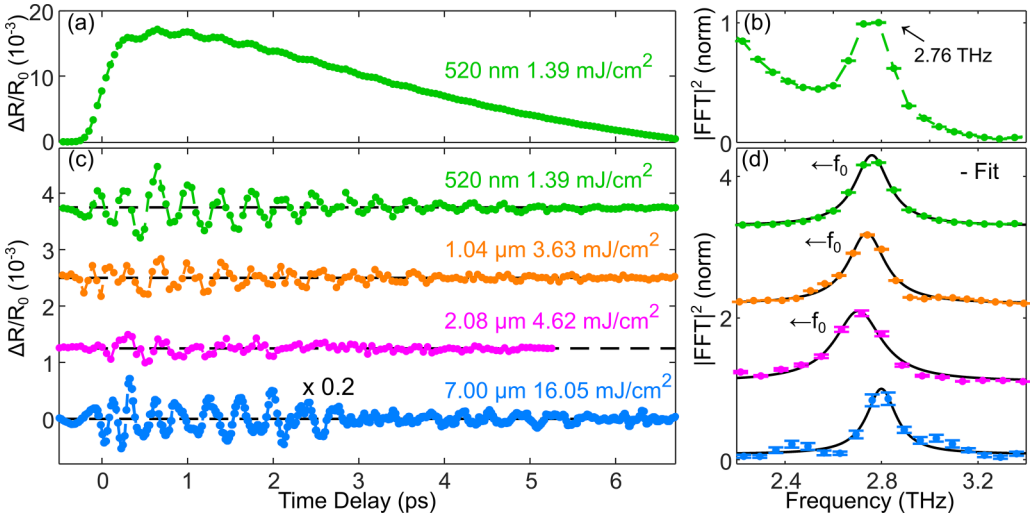

FIG. 2. (a) Dynamics of the normalized reflectivity of BiTeI induced by 520-nm laser pulses. The fluence was set to 1.39 mJ/cm^2. (b) Power spectrum of the time trace shown in panel (a), obtained via Fourier transform. (c) Oscillatory component of the transient reflectivity for pump wavelengths spanning the visible, near-infrared, and mid-infrared spectral ranges after subtraction of the incoherent background. For the 2.08-μm data (purple), the shorter coherence time (4.2 ps) allows us to limit the maximum scanned delay time to 5.3 ps, which improves the statistics while keeping the measurement time constant over the entire dataset shown in this figure. Note that for the 7.00-μm data (blue), the time trace was scaled with a factor of 0.2 for presentation purposes. (d) Power spectra of the time traces shown in panel (c). Each dataset is normalized on its peak value at the respective central frequency f_0. The solid black lines represent a fit with a Lorentzian function (details in [21]). For interband excitation (520 nm to 2.08 μm) f_0 redshifts with increasing fluence (see explanation in the main text).

oscillations is not steplike as indicated in Eq. (1) by $\Theta(t)$. This smooth onset and the removal of the incoherent background introduce complexity to the analysis in the time domain. Thus, we analyze the coherent component of the signal in the frequency domain (details in [21]). Since in the frequency domain the coherent component of $\Delta R(t)/R_0$ is narrow, the smooth onset has a negligible effect. The square of the absolute value of the Fourier transform of Eq. (1) for the frequencies $f > 0$ is given by

$$\left|\left(\frac{\Delta R(f)}{R_0}\right)_{\text{osci}}\right|^2 = \frac{(A_\text{o}\tau)^2}{8\pi}\frac{1}{1+4\pi^2\tau^2(f-f_0)^2} + c. \quad (2)$$

The parameter c was added to account for spectral offsets. By convention [29], we define the coherence time τ_c as the inverse spectral width Δf, where the spectral width is considered to be the full width at half maximum. Using Eq. (2) to find Δf, we conclude that the coherence time can be calculated from the lifetime via

$$\tau_\text{c} = \pi\tau. \quad (3)$$

To determine τ_c, we fit the power spectrum with Eq. (2). We find $\tau_\text{c} = 5.7 \pm 0.1$ ps. This result is in good agreement with the value obtained by spontaneous Raman scattering (6 ps) [20]. In contrast to the experiment reported in [20], however, we set the fluence Φ to a value that significantly increases the free-carrier density n_c. Our analysis shows that this has no effect on τ_c, which is at first surprising since LO phonons usually interact strongly with free electrons [30]. Driven by this finding, from Φ we calculate the excitation density, i.e., an estimate of the density of photons absorbed by electrons assuming that a single electron absorbs a single photon (details in [21]). We highlight that in the interband regime the excitation density is equal to the increase of n_c; i.e., the semiconductor is optically doped. This procedure results in $n_\text{c} \approx 4 \times 10^{20}$ cm^{-3}, a value almost one order of magnitude larger than the intrinsic charge-carrier density n_i. In comparison to III-V semiconductors (GaAs, GaP, InAs, InSb) [16–19], this behavior is remarkable. For example, in GaAs free carriers with a density three orders of magnitude smaller strongly suppress the coherence time of the lattice oscillations [19]. We attribute this difference to the van der Waals structure of BiTeI, due to which the electron wave vector is confined to the plane perpendicular to the stacking axis for states close to the conduction-band minimum. The wave vector of LO phonons with A_1 symmetry, however, is parallel to the stacking. Thus, the emission and absorption of such phonons by free electrons is suppressed due to the restrictions of energy and momentum conservation.

Motivated by this observation, we quantitatively analyze the phononic robustness with respect to the excitation density. For this purpose, we experimentally vary the pump fluence Φ. For each value of Φ we estimate the excitation density and analyze the amplitude A_o and the coherence time τ_c of the oscillations from the Lorentz fit (details in [21]). The results are shown in Figs. 3(a) and 3(b) by the green circles. The linear guide to the eye (dashed green line) suggests that the amplitude A_o of the phononic contribution to the signal [Fig. 3(a)] scales linearly with the excitation density. This is consistent with DECP [13]. We emphasize that Fig. 3(a) is plotted in double logarithmic scaling for the sake of presentation. In [21], we also show this plot in linear scaling. The value of τ_c [Fig. 3(b)], on the other hand, shows no significant density-dependent variations up to $n_\text{c} \approx 4 \times 10^{20}$ cm^{-3}.

Despite the scientific interest, we cannot further increase the fluence of the 520-nm pump beam, since the sample

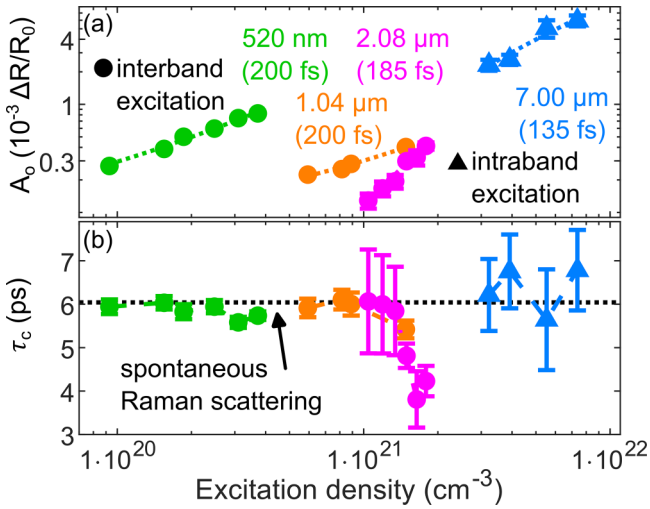

FIG. 3. Dependence of the phononic oscillation parameter on the excitation density. Pump wavelengths (pulse durations) are indicated in the top panel. The error bars represent the 95% confidence interval. (a) For each measurement series, the oscillation amplitude A_o shows a linear dependence on the excitation density. The data are plotted in a double-logarithmic scale for the sake of presentation, and the dotted lines represent linear guides to the eye. (b) Dependence of the coherence time τ_c on the excitation density. The value obtained via spontaneous Raman spectroscopy is shown by the dashed line [20].

damage threshold would be surpassed. We thus tune the central wavelength to 1.04 μm. The difference between excitation at 520 nm and 1.04 μm is that the excited electrons have less excess energy in the latter case (i.e., the energy difference between the excited state and the bottom of the conduction band). On the one hand, this allows us to further increase the fluence, as the damage threshold is higher compared to the 520-nm excitation. Therefore, we can analyze τ_c at even higher carrier densities. However, this also means that the electronic subsystem reaches a lower value of T_e after internal thermalization. This in turn allows us to investigate how the phononic amplitude A_o is affected when T_e is lower but n_c is comparable to the 520-nm excitation. We will first address the latter aspect. To begin with, with excitation at 1.04 μm we can increase the laser fluence to up to 3.63 mJ/cm^2, which corresponds to an excitation density of 1.5×10^{21} cm^{-3}. The oscillatory time trace of $\Delta R/R_0$ and the corresponding power spectrum measured at this highest fluence are shown in Figs. 2(c) and 2(d). The results of the excitation-density dependence analysis [orange circles in Figs. 3(a) and 3(b)] show that the amplitude A_o scales linearly with the excitation density as in the case of the 520-nm pump beam, however with smaller values. In fact, considering comparable values of the excitation density (4–6 $\times 10^{20}$ cm^{-3}), A_o is 3.6 times bigger in the dataset obtained with the 520-nm pump beam. Thus, we infer that the rise in T_e is indeed a major factor for DECP. With regard to τ_c we observe a reduction of the parameter value by about 10% at the highest excitation density (1.5×10^{21} cm^{-3}).

To further investigate the matter we set the pump-pulse central wavelength to 2.08 μm [purple in Figs. 2(c) and 2(d) and Figs. 3(a) and 3(b)]. In comparison to the 1.04-μm excitation, the values of A_o in the 2.08-μm data are lower, as expected, but the slope is bigger. This can be attributed to the different durations of the pump pulses, 200 fs at 1.04 μm compared to 185 fs at 2.08 μm. The closer the temporal profile of the excitation pulses is to a delta function, the more efficient DECP is [13].

As far as τ_c is concerned, a decrease down to 38% of the equilibrium value is observed at an excitation density of approximately 1.8×10^{21} cm^{-3} [see Fig. 3(b)], a value corresponding to $\Phi = 4.62$ mJ/cm^2. This decrease can also be seen in the time trace shown in Fig. 2(c) and in the broader power spectrum depicted in Fig. 2(d). Conversely, we have demonstrated that BiTeI can maintain the coherence time of the A_1 phonon mode up to an optically doped carrier density of $n_c \approx 1 \times 10^{21}$ cm^{-3}.

The eigenfrequency of the A_1 mode redshifts as the excitation density increases [see Fig. 2(d)]. It decreases by approximately 2% when comparing the values at the highest excitation densities between the 520-nm and 2.08-μm data. This renormalization of the lattice eigenfrequency stems from the screening of the ionic charges by the additional free charge carriers [31].

So far, we have demonstrated that BiTeI is phononically robust and that the rise in T_e plays a major role in DECP. However, pumping electronic interband transitions we could not completely disentangle the contribution of the rise in T_e from the increase of n_c to the phonon excitation. Therefore, we employ a pump beam in the mid-infrared range with a central wavelength of 7.00 μm. The corresponding photon energy (0.18 eV) is not high enough to induce interband excitation and thus cannot change n_c. However, mid-infrared pump pulses excite intraband transitions between the Rashba-split conduction bands [red arrow in Fig. 1(b)]. Consequently, we can further increase Φ in comparison to previous measurements without damaging the sample. In fact, we can employ fluences up to 16.1 mJ/cm^2, nearly four times higher than for 2.08-μm excitation and even one order of magnitude higher than for 520-nm excitation. This translates to excitation densities up to approximately 7.4×10^{21} cm^{-3}. We emphasize that the interpretation of the excitation density in the intraband regime is restricted to density of absorbed photons and explicitly does not include the simultaneous increase of n_c as in the interband regime. Nevertheless, the time-domain data [Fig. 2(c)] and the corresponding power spectrum [Fig. 2(d)] disclose that coherent phonons are excited even when n_c remains constant. Combined with the conclusions of electronic interband pumping, this compelling observation establishes that the rise in T_e and not the increase of n_c is the dominant contribution to DECP in BiTeI.

The amplitude retains its linear dependence on the fluence [blue triangles in Fig. 3(a)]. From the absence of nonlinearity in A_o, we conclude that a single photon excites a single electron for intraband excitation as well. A saturation of the amplitude due to bleaching of the electronic intraband transition could be expected, as the highest value for the excitation density is two orders of magnitude larger than n_i. However, photoexcited carriers in BiTeI scatter on a timescale shorter than 80 fs [28,32]. As the duration of the 7.00-μm pump pulses is 135 fs, the conduction-band electrons are redistributed in momentum space within the duration of the optical excitation, thus preventing the absorption from saturating.

In contrast to the interband regime, we observe that τ_c shows no significant excitation-density-dependent variations [blue triangles in Fig. 3(b)]. This can be attributed to the absence of additional scattering channels and energy dissipation mechanisms that typically arise with higher carrier densities. Therefore, pumping electronic intraband transitions selectively in BiTeI allows a linear increase of A_o with the fluence, while avoiding shortening τ_c. In addition, we observe that in contrast to the interband regime the frequency of the A_1 phonon is not affected [see Fig. 2(d)]. As the mid-infrared pulses cannot increase n_c, no screening of the ionic charges takes place.

Finally, we comment on the initial phase of the coherent-phonon oscillation. According to the standard DECP theory [9], a steplike displacement of the equilibrium coordinate of the ion cores results in cosine-like oscillations with a well-defined zero phase. This theoretical framework is experimentally applicable when the duration of the pump pulses is much shorter than the phonon oscillation period, ideally approximating a delta-function temporal profile [33–35]. In our experiment, however, this condition is not satisfied, as the pump-pulse duration (200 fs) is almost comparable to the phonon oscillation period (360 fs). Consequently, the onset of the lattice equilibrium-coordinate displacement is temporally broadened, and the observed oscillations deviate from the ideal cosine-like behavior with zero-phase temporal dependence. This aspect is discussed in greater detail in [21], where we also demonstrate how a finite pump-pulse duration affects the oscillation onset within the framework of DECP theory [9]. Notably, the impact of the excitation's temporal profile on the phase of the observed oscillations has also been investigated using alternative theoretical models [36].

Conclusion. We have demonstrated displacive excitation of coherent phonons in BiTeI. By tuning the pump central wavelength in a broad spectral range spanning the visible, near-infrared, and even mid-infrared regimes we observe DECP for both electronic interband and intraband transitions. In the former scenario, we find that the phonon coherence time can be maintained for charge-carrier densities up to $n_c = 1 \times 10^{21}$ cm^{-3}. This demonstrates a remarkable phononic robustness, since in III-V semiconductors the coherence time is already suppressed at values of n_c orders of magnitude lower. The scenario of intraband transitions has been so far barely explored in terms of DECP. Our data demonstrate that the photoinduced rise of T_e is the main microscopic contribution to DECP. Furthermore, in this regime we can raise the phononic amplitude by increasing the fluence, while the coherence time is unaffected. We observe that these results may be relevant for the development of optically driven ultrafast technology in quantum materials. Schemes addressing the coherent structural manipulation of solids can be based on exciting electronic intraband transitions selectively, thus avoiding the additional scattering channels and energy dissipation induced by an increase of the carrier density. Other routes, like Raman sum-frequency generation [37] and nonlinear phononics [38], are expected to induce the same phonon modes even in a nonlinear dynamical regime. This is relevant with regard to the symmetry of the 2.7 THz mode, which may allow direct modification of the Rashba coupling [39–44].

Acknowledgments. The exchange of samples took place in May 2021. The authors thank C. Beschle and S. Eggert for their technical support. This work was supported by the Deutsche Forschungsgemeinschaft (DFG; Program No. BO 5074/2-1). D.B. acknowledges also the support of DFG Program No. BO 5074/1-1.

[1] K. W. Kim, A. Pashkin, H. Schäfer, M. Beyer, M. Porer, T. Wolf, C. Bernhard, J. Demsar, R. Huber, and A. Leitenstorfer, Ultrafast transient generation of spin-density-wave order in the normal state of $BaFe_2As_2$ driven by coherent lattice vibrations, Nat. Mater. **11**, 497 (2012).

[2] T. F. Nova, A. Cartella, A. Cantaluppi, M. Först, D. Bossini, R. V. Mikhaylovskiy, A. V. Kimel, R. Merlin, and A. Cavalleri, An effective magnetic field from optically driven phonons, Nat. Phys. **13**, 132 (2017).

[3] T. F. Nova, A. S. Disa, M. Fechner, and A. Cavalleri, Metastable ferroelectricity in optically strained $SrTiO_3$, Science **364**, 1075 (2019).

[4] D. Fausti, R. I. Tobey, N. Dean, S. Kaiser, A. Dienst, M. C. Hoffmann, S. Pyon, T. Takayama, H. Takagi, and A. Cavalleri, Light-induced superconductivity in a stripe-ordered cuprate, Science **331**, 189 (2011).

[5] S. Wall, D. Wegkamp, L. Foglia, K. Appavoo, J. Nag, R. Haglund, J. Stähler, and M. Wolf, Ultrafast changes in lattice symmetry probed by coherent phonons, Nat. Commun. **3**, 721 (2012).

[6] F. Mertens, D. Mönkebüscher, U. Parlak, C. Boix-Constant, S. Mañas-Valero, M. Matzer, R. Adhikari, A. Bonanni, E. Coronado, A. M. Kalashnikova, D. Bossini, and M. Cinchetti, Ultrafast coherent THz lattice dynamics coupled to spins in the van der Waals antiferromagnet $FePS_3$, Adv. Mater. **35**, 2208355 (2023).

[7] T. K. Cheng, S. D. Brorson, A. S. Kazeroonian, J. S. Moodera, G. Dresselhaus, M. S. Dresselhaus, and E. P. Ippen, Impulsive excitation of coherent phonons observed in reflection in bismuth and antimony, Appl. Phys. Lett. **57**, 1004 (1990).

[8] G. C. Cho, W. Kütt, and H. Kurz, Subpicosecond time-resolved coherent-phonon oscillations in GaAs, Phys. Rev. Lett. **65**, 764 (1990).

[9] H. J. Zeiger, J. Vidal, T. K. Cheng, E. P. Ippen, G. Dresselhaus, and M. S. Dresselhaus, Theory for displacive excitation of coherent phonons, Phys. Rev. B **45**, 768 (1992).

[10] E. D. Murray, D. M. Fritz, J. K. Wahlstrand, S. Fahy, and D. A. Reis, Effect of lattice anharmonicity on high-amplitude phonon dynamics in photoexcited bismuth, Phys. Rev. B **72**, 060301(R) (2005).

[11] D. M. Fritz, D. A. Reis, B. Adams, R. A. Akre, J. Arthur, C. Blome, P. H. Bucksbaum, A. L. Cavalieri, S. Engemann, S. Fahy, R. W. Falcone, P. H. Fuoss, K. J. Gaffney, M. J. George, J. Hajdu, M. P. Hertlein, P. B. Hillyard, M. Horn-von Hoegen, M. Kammler, J. Kaspar *et al.*, Ultrafast bond softening in bismuth: Mapping a solid's interatomic potential with x-rays, Science **315**, 633 (2007).

[12] F. Giorgianni, M. Udina, T. Cea, E. Paris, M. Caputo, M. Radovic, L. Boie, J. Sakai, C. W. Schneider, and S. L. Johnson,

Terahertz displacive excitation of a coherent Raman-active phonon in V_2O_3, Commun. Phys. **5**, 103 (2022).
[13] R. Merlin, Generating coherent THz phonons with light pulses, Solid State Commun. **102**, 207 (1997).
[14] T. E. Stevens, J. Kuhl, and R. Merlin, Coherent phonon generation and the two stimulated Raman tensors, Phys. Rev. B **65**, 144304 (2002).
[15] A. A. Makhnev, L. V. Nomerovannaya, T. V. Kuznetsova, O. E. Tereshchenko, and K. A. Kokh, Optical properties of BiTeI semiconductor with a strong Rashba spin-orbit interaction, Opt. Spectrosc. **117**, 764 (2014).
[16] W. Kutt, G. C. Cho, T. Pfeifer, and H. Kurz, Subpicosecond generation and decay of coherent phonons in III-V compounds, Semicond. Sci. Technol. **7**, B77 (1992).
[17] O. V. Misochko, Coherent phonons and their properties, J. Exp. Theor. Phys. **92**, 246 (2001).
[18] K. J. Yee, K. G. Lee, E. Oh, D. S. Kim, and Y. S. Lim, Coherent optical phonon oscillations in bulk GaN excited by far below the band gap photons, Phys. Rev. Lett. **88**, 105501 (2002).
[19] M. Hase, S.-I. Nakashima, K. Mizoguchi, H. Harima, and K. Sakai, Ultrafast decay of coherent plasmon-phonon coupled modes in highly doped GaAs, Phys. Rev. B **60**, 16526 (1999).
[20] I. Y. Sklyadneva, R. Heid, K.-P. Bohnen, V. Chis, V. A. Volodin, K. A. Kokh, O. E. Tereshchenko, P. M. Echenique, and E. V. Chulkov, Lattice dynamics of bismuth tellurohalides, Phys. Rev. B **86**, 094302 (2012).
[21] See Supplemental Material at http://link.aps.org/supplemental/10.1103/PhysRevB.111.L081201 for details concerning the laser system, the analysis of the electronic background and the coherent oscillations, and the optical parameters of BiTeI.
[22] C. Schoenfeld, L. Feuerer, A. Heinrich, A. Leitenstorfer, and D. Bossini, Nonlinear generation, compression and spatio-temporal analysis of sub-GV/cm-class femtosecond mid-infrared transients, Laser Photon. Rev. **18**, 2301152 (2024).
[23] K. Ishizaka, M. S. Bahramy, H. Murakawa, M. Sakano, T. Shimojima, T. Sonobe, K. Koizumi, S. Shin, H. Miyahara, A. Kimura, K. Miyamoto, T. Okuda, H. Namatame, M. Taniguchi, R. Arita, N. Nagaosa, K. Kobayashi, Y. Murakami, R. Kumai, Y. Kaneko *et al.*, Giant Rashba-type spin splitting in bulk BiTeI, Nat. Mater. **10**, 521 (2011).
[24] E. Rashba, Semiconductors with a loop of extrema, J. Electron Spectrosc. Relat. Phenom. **201**, 4 (2015).
[25] L. Demkó, G. A. H. Schober, V. Kocsis, M. S. Bahramy, H. Murakawa, J. S. Lee, I. Kézsmárki, R. Arita, N. Nagaosa, and Y. Tokura, Enhanced infrared magneto-optical response of the nonmagnetic semiconductor BiTeI driven by bulk Rashba splitting, Phys. Rev. Lett. **109**, 167401 (2012).
[26] M. S. Bahramy, R. Arita, and N. Nagaosa, Origin of giant bulk Rashba splitting: Application to BiTeI, Phys. Rev. B **84**, 041202(R) (2011).
[27] J. S. Lee, G. A. H. Schober, M. S. Bahramy, H. Murakawa, Y. Onose, R. Arita, N. Nagaosa, and Y. Tokura, Optical response of relativistic electrons in the polar BiTeI semiconductor, Phys. Rev. Lett. **107**, 117401 (2011).
[28] A. S. Ketterl, B. Andres, M. Polverigiani, V. Voroshnin, C. Gahl, K. A. Kokh, O. E. Tereshchenko, E. V. Chulkov, A. Shikin, and M. Weinelt, Effect of Rashba splitting on ultrafast carrier dynamics in BiTeI, Phys. Rev. B **103**, 085406 (2021).
[29] R. Loudon, *The Quantum Theory of Light*, 3rd ed. (Oxford University Press, Oxford, 2000).
[30] H. Fröhlich, Electrons in lattice fields, Adv. Phys. **3**, 325 (1954).
[31] P. Yu and M. Cardona, *Fundamentals of Semiconductors*, 3rd ed. (Springer, Berlin, 2005).
[32] J. Mauchain, Y. Ohtsubo, M. Hajlaoui, E. Papalazarou, M. Marsi, A. Taleb-Ibrahimi, J. Faure, K. A. Kokh, O. E. Tereshchenko, S. V. Eremeev, E. V. Chulkov, and L. Perfetti, Circular dichroism and superdiffusive transport at the surface of BiTeI, Phys. Rev. Lett. **111**, 126603 (2013).
[33] T. K. Cheng, J. Vidal, H. J. Zeiger, G. Dresselhaus, M. S. Dresselhaus, and E. P. Ippen, Mechanism for displacive excitation of coherent phonons in Sb, Bi, Te, and Ti_2O_3, Appl. Phys. Lett. **59**, 1923 (1991).
[34] G. A. Garrett, T. F. Albrecht, J. F. Whitaker, and R. Merlin, Coherent THz phonons driven by light pulses and the Sb problem: What is the mechanism? Phys. Rev. Lett. **77**, 3661 (1996).
[35] M. Hase, K. Mizoguchi, H. Harima, S.-I. Nakashima, and K. Sakai, Dynamics of coherent phonons in bismuth generated by ultrashort laser pulses, Phys. Rev. B **58**, 5448 (1998).
[36] C. Giannetti, B. Revaz, F. Banfi, M. Montagnese, G. Ferrini, F. Cilento, S. Maccalli, P. Vavassori, G. Oliviero, E. Bontempi, L. E. Depero, V. Metlushko, and F. Parmigiani, Thermomechanical behavior of surface acoustic waves in ordered arrays of nanodisks studied by near-infrared pump-probe diffraction experiments, Phys. Rev. B **76**, 125413 (2007).
[37] D. M. Juraschek and S. F. Maehrlein, Sum-frequency ionic Raman scattering, Phys. Rev. B **97**, 174302 (2018).
[38] M. Först, Y. Tokura, C. Manzoni, S. Kaiser, Y. Tomioka, R. Merlin, R. Merlin, and A. Cavalleri, Nonlinear phononics as an ultrafast route to lattice control, Nat. Phys. **7**, 854 (2011).
[39] A. Crepaldi, L. Moreschini, G. Autès, C. Tournier-Colletta, S. Moser, N. Virk, H. Berger, P. Bugnon, Y. J. Chang, K. Kern, A. Bostwick, E. Rotenberg, O. V. Yazyev, and M. Grioni, Giant ambipolar Rashba effect in the semiconductor BiTeI, Phys. Rev. Lett. **109**, 096803 (2012).
[40] L. Cheng, L. Wei, H. Liang, Y. Yan, G. Cheng, M. Lv, T. Lin, T. Kang, G. Yu, J. Chu, Z. Zhang, and C. Zeng, Optical manipulation of Rashba spin-orbit coupling at $SrTiO_3$-based oxide interfaces, Nano Lett. **17**, 6534 (2017).
[41] G. Kremer, J. Maklar, L. Nicolaï, C. W. Nicholson, C. Yue, C. Silva, P. Werner, J. H. Dil, J. Krempaský, G. Springholz, R. Ernstorfer, J. Minár, L. Rettig, and C. Monney, Field-induced ultrafast modulation of Rashba coupling at room temperature in ferroelectric α-GeTe(111), Nat. Commun. **13**, 6396 (2022).
[42] S. T. Ciocys, N. Maksimovic, J. G. Analytis, and A. Lanzara, Driving ultrafast spin and energy modulation in quantum well states via photo-induced electric fields, npj Quantum Mater. **7**, 79 (2022).
[43] M. Michiardi, F. Boschini, H.-H. Kung, M. X. Na, S. K. Y. Dufresne, A. Currie, G. Levy, S. Zhdanovich, A. K. Mills, D. J. Jones, J. L. Mi, B. B. Iversen, P. Hofmann, and A. Damascelli, Optical manipulation of Rashba-split 2-dimensional electron gas, Nat. Commun. **13**, 3096 (2022).
[44] J. Qu, E. F. Cuddy, X. Han, J. Liu, H. Li, Y.-J. Zeng, B. Moritz, T. P. Devereaux, P. S. Kirchmann, Z.-X. Shen, and J. A. Sobota, Screening of polar electron-phonon interactions near the surface of the Rashba semiconductor BiTeCl, Phys. Rev. Lett. **133**, 106401 (2024).